Energy 113 (2016) 248–257

Contents lists available at ScienceDirect

Energy

journal homepage: www.elsevier.com/locate/energy

Nonlinear observer-based control for PMSG wind turbine

Roberto Fantino, Jorge Solsona*, Claudio Busada

Instituto de Investigaciones en Ingeniería Eléctrica (IIIE) "Alfredo Desages" (UNS-CONICET), Departamento de Ingeniería Eléctrica y de Computadoras, Universidad Nacional del Sur (UNS), 8000, Bahía Blanca, Argentina

ARTICLE INFO

Article history:
Received 11 December 2015
Received in revised form
30 June 2016
Accepted 7 July 2016

Keywords:
Permanent magnet synchronous generator
WECS
Sensorless control
Nonlinear observer
MPPT

ABSTRACT

This paper introduces a mechanical sensorless control strategy to be used in variable speed wind energy conversion systems based on permanent magnet synchronous generators. The goal of the control strategy is to track the wind turbine maximum power point. With the proposed strategy, mechanical sensors are not needed to implement the control law. For this reason, electrical sensors -voltage and current sensors-are only needed to build the control law.

In order to obtain estimates of the mechanical variables, a nonlinear Luenberger-like observer is designed. This observer only uses measurements of the electrical variables. The estimates are fed back to the controller in order to build the mechanical sensorless control strategy.

The performance of the whole system is tested through simulations.

1. Introduction

Wind energy conversion systems (WECS) used in distributed generation must be able to inject energy in an efficient way. To this end, nowadays, the use of speed variable permanent magnet synchronous generator (PMSG) has increased a lot. It is mainly because PMSGs based WECSs have high efficiency and they reduce operation and maintenance cost, since this scheme does not employ neither gearbox nor slip rings. In addition, PMSGs based WECSs can be controlled for wind turbine maximum power point transfer (MPPT) operation, in a wide range of the wind speeds [1,2].

In order to transfer power from the generator to the grid, most of WECSs include Voltage Source Converters (VSCs). However, over the last few years, the use of topologies including Current Source Converters (CSCs) have increased a lot. This is because these topologies present several advantages [3,4]: 1) natural protection against shortcircuit 2) low dv/dt variations of the output voltage 3) high reliability of conversion and 4) regenerative capacity [5]. There are different configurations for WECS based on CSCs. One of the best, when it comes to power quality, consists of a current source rectifier (CSR) and a current source inverter (CSI) connected in a back-to-back configuration [6–8].

Many times, when the turbine power coefficient ($C_p(\lambda,\beta)$) is known, the power can be controlled to track the maximum power point. To this end, control algorithms for MPPT operation are implemented (see for instance, [9–12] and references therein). In such a case, the PMSG torque must be controlled [13–16] by setting the torque reference as a function of the mechanical variables. It is possible to measure mechanical variables to implement the control strategy. Nevertheless, in order to reduce cost and to increase the system reliability, sensorless algorithms can be used to estimate them. It can be mentioned that in Ref. [17], many of the problems that must be solved in order to obtain a more reliable and smart wind energy system were identified. There, optimum control strategies for PMSG wind turbine systems without mechanical sensors are mentioned. Some researchers have already proposed mechanical sensorless strategies. For instance, in Refs. [15,18] a PLL is used to estimate the turbine speed and the rotor speed. This strategy does not consider the acceleration in its prediction model. However, including the acceleration in the prediction model improves the estimator transient performance, and therefore, it is included in the proposal of this manuscript. In Ref. [19] a low-pass filter is used to estimate the stator flux, and then the mechanical speed is estimated via a recursive LMS algorithm. In Ref. [14] the stator flux and the rotor mechanical speed are estimated with a quasi sliding mode observer. In Ref. [20] a sliding mode observer estimates both the rotor speed and the rotor position. In other proposals these variables are estimated by using adaptive reference models (see Refs. [21,22]). Sliding-observers can be considered as linear high gain observers where the correction term introduces a

* Corresponding author. DIEC – UNS, Av. Alem 1253, 8000, Bahía Blanca, Argentina.
E-mail address: jsolsona@uns.edu.ar (J. Solsona).

http://dx.doi.org/10.1016/j.energy.2016.07.039
0360-5442/

constant high gain. These observers present chattering. For this reason, the estimated position is obtained from filtered EMF. The low pass filter used to filter the EMF deteriorates the system performance. Our proposal, introduces a correction term where a nonlinear gain is used to guarantee the convergence of the estimation error and improve the observer performance. In Ref. [23] the authors propose a method for wind speed estimation. The mechanical torque is approximated by using a neural network identifier. Our proposal uses a simple technique for the estimation of the mechanical torque. In Ref. [24] a sensorless control scheme for PMSG with diode bridge rectifier is presented. In this scheme, when parameters change, the system does not work in the maximum power point. For this reason, in Refs. [25], the authors analyze the system behavior under this undesirable condition. In our scheme, it is assumed that in order to obtain the maximum power transfer, the control strategy is calculated to track the maximum power point. In Ref. [26] an algebraic estimator is used. It must be noted that in this case, fast transients can make the system unstable. In our proposal, the dynamic model of the PMSG is considered in the design of the estimation algorithm. In Ref. [27] an unscented Kalman filter algorithm is proposed. This algorithm is based on Taylor's linearization technique. Our estimator design is based on a nonlinear technique. It is well-known that Taylor's linearization guarantees convergence in a small region around the equilibrium point. However, the PMSG model is highly nonlinear. For this reason is better to use a nonlinear technique to build the estimator, such as it is proposed in this work.

In this work a mechanical sensorless strategy for controlling a WECS consisting of a wind turbine, a PMSG and two CSCs connected in a back-to-back configuration is proposed. The control strategy is designed for MPPT operation by controlling the PMSG torque. The controller uses estimates of the rotor speed, rotor position and the PMSG electrical torque. The estimates are obtained via a nonlinear observer [28]. This observer uses the measurement of the electrical variables. The proposed nonlinear observer consists of two terms. The first term copies the system dynamics. This is the prediction term. A correction term is added to the prediction term. The correction term includes a nonlinear gain matrix. This paper contains a criterion for designing the nonlinear gain matrix. Simulation results are presented in order to show the performance of the whole system.

The rest of the paper is organized as follows. In Section 2, the system is described. The PMSG model and the nonlinear observer used to estimate the mechanical variables are introduced in Section 3. Section 4 contains a brief description of the wind turbine model and the MPPT control method. Different simulation tests for validating the system performance are included in Section 5. Finally, conclusions are drawn in Section 6, and the criterion for designing the observer's nonlinear gain matrix is presented in the Appendix section at the end of this paper.

2. System description

In Fig. 1 the WECS under study is shown. The turbine and PMSG axles are directly coupled (no gearbox is used), consequently both axles rotate to the same speed (ω_m). The wind power captured by the turbine is transformed into electrical power by the PMSG. Then, this energy is transferred to the grid via a power conversion system. This power conversion system consists of two three-phase current converters connected in a back-to-back configuration with a coupling inductor (L_{dc}) [29]. The generator side converter works as a CSR [1,29], controlling the power flux extracted from the turbine and transferred to the grid. The grid side converter works as a CSI [1,29], converting the energy stored in L_{dc}, in a three phase current synchronized with the grid voltage. Both converters operate with Space Vector Modulation (SVM) [1,29,30]; m_G and θ_G represent, the modulation index and the reference angle, respectively, used to control the CSR modulation. Whereas, m_R and θ_R represent the modulation index and the reference angle used to control the CSI modulation.

Since the current high frequency components flowing to the generator must be attenuated, the CSR and the PMSG are connected through an LC filter (LC_R in Fig. 1). The same concept is used for connecting the CSI and the grid (see LC_I). In order to implement the CSI controller, three phase grid voltage $v_{R_{abc}}$, three phase grid current $i_{R_{abc}}$ and DC-link voltage V_{dc} (in the rectifier side) are measured, as shown in Fig. 1. It must be remarked that the CSI control is not the focus of this paper. For this reason, a simple control scheme for injecting current satisfying unity power factor condition is used. However, it is possible to design another strategy. For instance, a strategy proposing to inject reactive power to the grid could be employed [1,29,31]. The three phase measurements are transformed into a two-axes reference frame $\alpha\beta$. The grid voltage, in this new reference frame ($v_{R_{\alpha\beta}}$), is transformed into polar coordinates and is represented by its magnitude $|v_R|$ and its angle θ_{v_R}. The CSI-SVM uses the modulation index $m_R = V_{dc}/|v_R|$ as reference [1].

It must be noted that the grid and inverter output currents are not in-phase, because the LC_R filter introduces a phase shift. In order to correct this deviation, CSI reference angle θ_R is calculated adding grid voltage angle θ_{v_R} and a PI controller output, whose input is the cross product between current and voltage vectors ($i_{\alpha\beta} \times v_{\alpha\beta}$). This product is equal to zero when the current and voltage are in-phase. A saturation block limits the PI output to $-\pi/2<\theta<\pi/2$.

The CSR controller uses the measurements of the generator currents and voltages (i.e. $v_{G_{abc}}$ and $i_{G_{abc}}$, respectively). The control law is to be calculated in the $\alpha\beta$ reference frame. For this reason, the measurements are transformed into the $\alpha\beta$ reference frame by using the Clarke's transformation. In this way, variables $v_{G_{\alpha\beta}}$ and $i_{G_{\alpha\beta}}$ are obtained.

The goal of the “MPPT Control” block is make the turbine operate on the curve corresponding to the maximum power point transfer (MPPT) [1]. To this end, PMSG electrical torque T_e will be controlled to achieve that the turbine axle rotates to the optimal speed, irrespectively of the wind speed value. In order to obtain a good performance, the following variables should be fed back to the MPPT controller: the PMSG rotor speed (ω_m), the PMSG rotor position (θ_m) and the PMSG electrical torque (T_e). Nevertheless, it is very important to remark that in our proposal, mechanical sensors will be avoided with minimal performance impact. To this end, estimated values of the rotor speed, the rotor position and the electrical torque ($\widehat{\omega}_m$, $\widehat{\theta}_m$ and $\widehat{T}_e$) will be obtained through a nonlinear observer [28], whose inputs are the electrical variables $v_{G_{\alpha\beta}}$ and $i_{G_{\alpha\beta}}$ (see block “Obs.” in Fig. 1).

3. PMSG model and nonlinear observer

In $\alpha\beta$ reference frame, the non-salient pole PMSG model is described as [27]:

$$\begin{cases} \dfrac{di_{G_\alpha}}{dt} = -\dfrac{R}{L} i_{G_\alpha} - \dfrac{\lambda_M}{L} P\omega_m \sin(P\theta_m) - \dfrac{1}{L} v_{G_\alpha}, \\ \dfrac{di_{G_\beta}}{dt} = -\dfrac{R}{L} i_{G_\beta} + \dfrac{\lambda_M}{L} P\omega_m \cos(P\theta_m) - \dfrac{1}{L} v_{G_\beta}, \\ \dfrac{d\theta_m}{dt} = \omega_m, \\ \dfrac{d\omega_m}{dt} = \dfrac{1}{J} T_m - \dfrac{1}{J} T_e - \dfrac{B}{J} \omega_m, \end{cases} \tag{1}$$

with

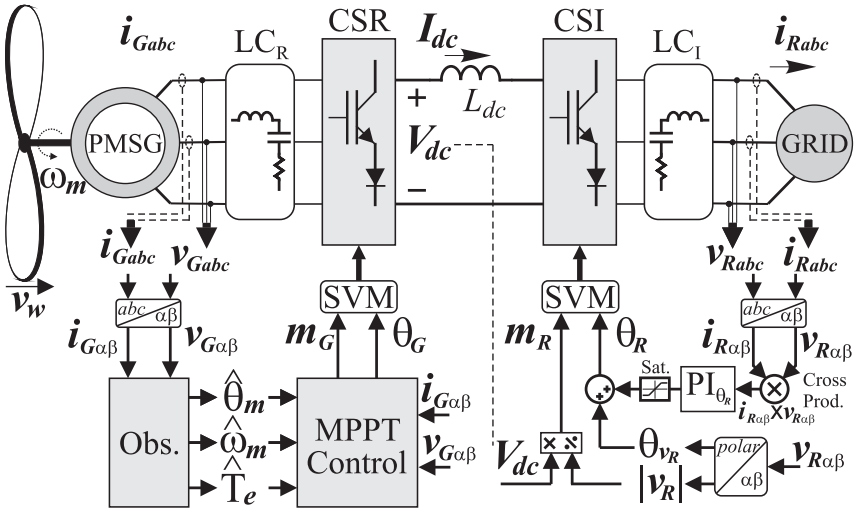

Fig. 1. Wind energy conversion system.

$$T_e = \frac{3}{2} P \lambda_M \left[- i_{G_\alpha} \sin(P\theta_m) + i_{G_\beta} \cos(P\theta_m) \right], \tag{2}$$

where i_{G_α}, i_{G_β}, v_{G_α}, v_{G_β}, R and L are the generator currents and voltages in $\alpha\beta$ reference frame; the stator resistance and inductance, respectively. λ_M is the rotor permanent magnet concatenated flux; θ_m and ω_m are the rotor position and speed; T_m is the turbine mechanical torque applied to the generator rotor, and T_e is the generator electrical torque; P is the number of pole pairs; J and B are the moment of inertia and viscosity coefficients of the combined turbine-generator set. An extended nonlinear observer [28] is used to estimate the mechanical variables (ω_m, θ_m) and the generator electrical torque (T_e) (see block "Obs." in Fig. 1). The observer consists of two terms. The prediction term copies the PMSG dynamic model and the correction term uses the measured currents $i_{G_{\alpha\beta}}$. In order to avoid to use a torquemeter, turbine torque T_m is added to the model (Eqn. (1)) as a new state that will be estimated by the nonlinear observer. By assuming that the torque dynamics is slow, its dynamic model results:

$$\frac{dT_m}{dt} \simeq 0. \tag{3}$$

The extended nonlinear observer is given by Ref. [28]:

$$\begin{bmatrix} \frac{d\hat{\theta}_m}{dt} \\ \frac{d\hat{\omega}_m}{dt} \\ \frac{d\hat{i}_{G_\alpha}}{dt} \\ \frac{d\hat{i}_{G_\beta}}{dt} \\ \frac{d\hat{T}_m}{dt} \end{bmatrix} = \begin{bmatrix} \hat{\omega}_m \\ \frac{\hat{T}_m}{J} - \frac{B\hat{\omega}_m}{J} - \frac{3P}{2J}\lambda_M \left[- \hat{i}_{G_\alpha} \sin\left(P\hat{\theta}_m\right) + \hat{i}_{G_\beta} \cos\left(P\hat{\theta}_m\right) \right] \\ -\frac{R}{L}\hat{i}_{G_\alpha} - \frac{\lambda_M}{L} P\hat{\omega}_m \sin\left(P\hat{\theta}_m\right) - \frac{1}{L} v_{G_\alpha} \\ -\frac{R}{L}\hat{i}_{G_\beta} + \frac{\lambda_M}{L} P\hat{\omega}_m \cos\left(P\hat{\theta}_m\right) - \frac{1}{L} v_{G_\beta} \\ 0 \end{bmatrix} + \Upsilon \begin{bmatrix} \left(i_{G_\alpha} - \hat{i}_{G_\alpha}\right) \\ \left(i_{G_\beta} - \hat{i}_{G_\beta}\right) \end{bmatrix}, \tag{4}$$

with

$$\Upsilon = \begin{bmatrix} \Gamma G \\ k_1 \sin\left(P\hat{\theta}_m\right) \quad -k_2 \cos\left(P\hat{\theta}_m\right) \end{bmatrix}, G = \begin{bmatrix} g_{11} & g_{12} \\ g_{21} & g_{22} \\ g_{31} & g_{32} \\ g_{41} & g_{42} \end{bmatrix}, \Gamma = \begin{bmatrix} \frac{-L}{\lambda_M} \frac{\cos\left(P\hat{\theta}_m\right)}{P\hat{\omega}_m} & \frac{-L}{\lambda_M} \frac{\sin\left(P\hat{\theta}_m\right)}{P\hat{\omega}_m} & 0 & 0 \\ \frac{-L}{\lambda_M} \sin\left(P\hat{\theta}_m\right) & \frac{L}{\lambda_M} \cos\left(P\hat{\theta}_m\right) & 0 & 0 \\ 0 & 0 & 1 & 0 \\ 0 & 0 & 0 & 1 \end{bmatrix},$$

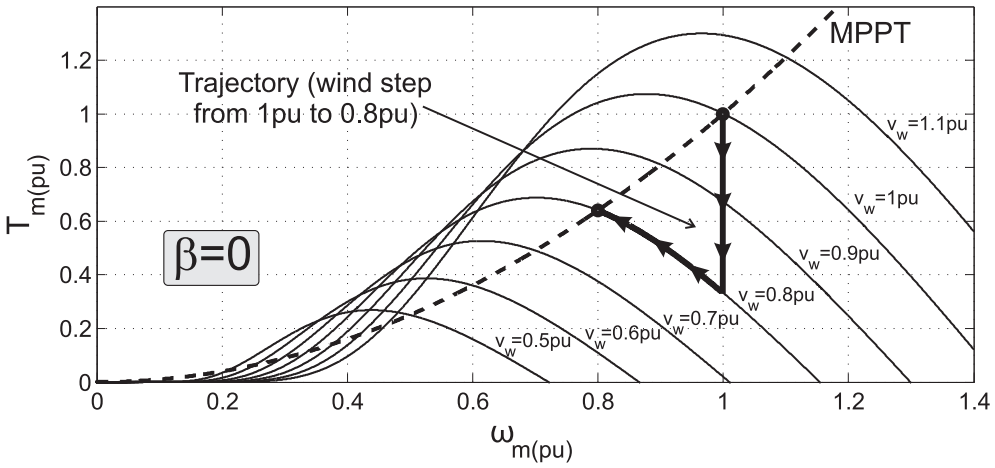

Fig. 2. T_m Vs. ω_m Curve (in pu) for several wind speeds v_w, and maximum power curve.

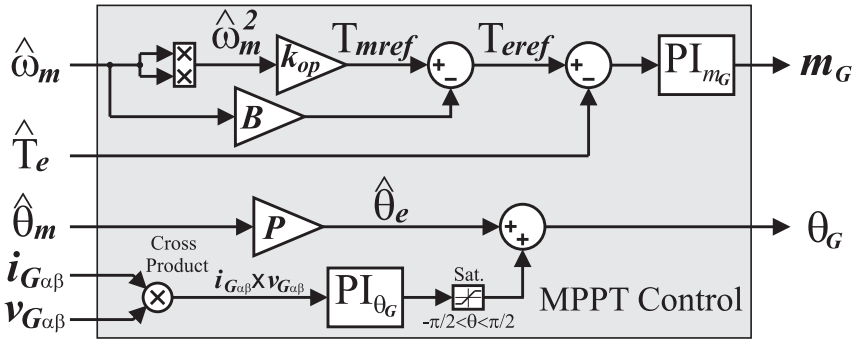

Fig. 3. MPPT control.

Table 1
PMSG, Wind Turbine and Observer parameters.

PMSG[32]	$P_{m_{nom}} = 10kW$; $T_{m_{nom}} = 137.88Nm$; $\omega_{m_{nom}} = 72.52rad/s$; $P = 19$; $R = 0.5\Omega$; $L = 4.48mHy$; $\lambda_M = 0.39Wb$; $J = 0.5Kgm^2$; $B = 0.03Nms/rad$;
Turbine	$C_{p_{nom}} = 0.44$; $\lambda_{nom} = 5.9$; $\beta = 0$; $v_{w_{nom}} = 12m/s$; $K_{opt} = 0.1316$
ObserverGains	$g11 = 2 \times 106$; $g12 = g22 = 2 \times 105$; $g21 = g32 = g41 = 0$; $g31 = g42 = 2 \times 10^3$; $k1 = k2 = -5 \times 10^5$

Table 2
WECS parameters and PI controllers gains.

Grid	VRLL = 381Vrms; fR = 50 Hz
CSR–CSI	fSVM = 10 kHz; Ldc = 10 mHy
LCR	LR = 3 mHy; CR = 5 μF; RR = 4 Ω
LCI	LI = 1 mHy; CI = 5 μF; RI = 1 Ω
PI_{θ_R}	$K_{P_{\theta_R}} = 1 \times 10^{-4}$; $K_{I_{\theta_R}} = 5 \times 10^{-2}$
PI_{θ_G}	$K_{P_{\theta_G}} = 1 \times 10^{-4}$; $K_{I_{\theta_G}} = 5 \times 10^{-2}$
PI_{m_G}	$K_{P_{m_G}} = 1 \times 10^{-3}$; $K_{I_{m_G}} = 0.4$

where $\widehat{\omega}_m$, $\widehat{\theta}_m$, $\widehat{i}_{G_\alpha}$ and $\widehat{i}_{G_\beta}$ stand for the estimation of the generator states defined in (1) and $\widehat{T}_m$ represents the estimated mechanical torque. By replacing estimated rotor position $\widehat{\theta}_m$ in Eqn. (2) and using calculated currents i_{G_α} and i_{G_β}, it is possible to estimate the electrical torque as:

$$\widehat{T}_e = \frac{3}{2} P \lambda_M \left[-i_{G_\alpha} \sin\left(P\widehat{\theta}_m\right) + i_{G_\beta} \cos\left(P\widehat{\theta}_m\right) \right]. \quad (5)$$

In the Appendix at the end of this paper the method used to obtain the observer's gain matrix Υ is presented.

4. Wind turbine model and MPPT control

The extracted wind power by a horizontal axle turbine can be calculated as [1]:

$$P_m = 0.5\pi\rho C_p(\lambda,\beta) r^2 v_w^3, \quad (6)$$

where r represents the wind turbine blade radius, v_w represents the wind speed, ρ represents the air density, λ is a coefficient including the tip speed of blade and wind speed rate. This coefficient is given by $\lambda = \omega_m r / v_w$. β represents the pitch angle and $C_p(\lambda,\beta)$ is the turbine power coefficient. The turbine transfers into the generator a mechanical power P_m. As a consequence, the mechanical torque applied by the turbine results $T_m = P_m/\omega_m$. Fig. 2 illustrates (in per unity (pu)), the curves of mechanical torque as a function of ω_m, and parameterized as a function of the wind speed, for $\beta = 0$. For each v_w value, the maximum extracted power is a function of ω_m. Then, in order to extract the maximum power of the wind turbine, the mechanical torque must track the maximum power curve (dashed curve in Fig. 2). Then, the optimal torque value becomes:

$$T_{m_{opt}} = K_{opt} \omega_m^2. \quad (7)$$

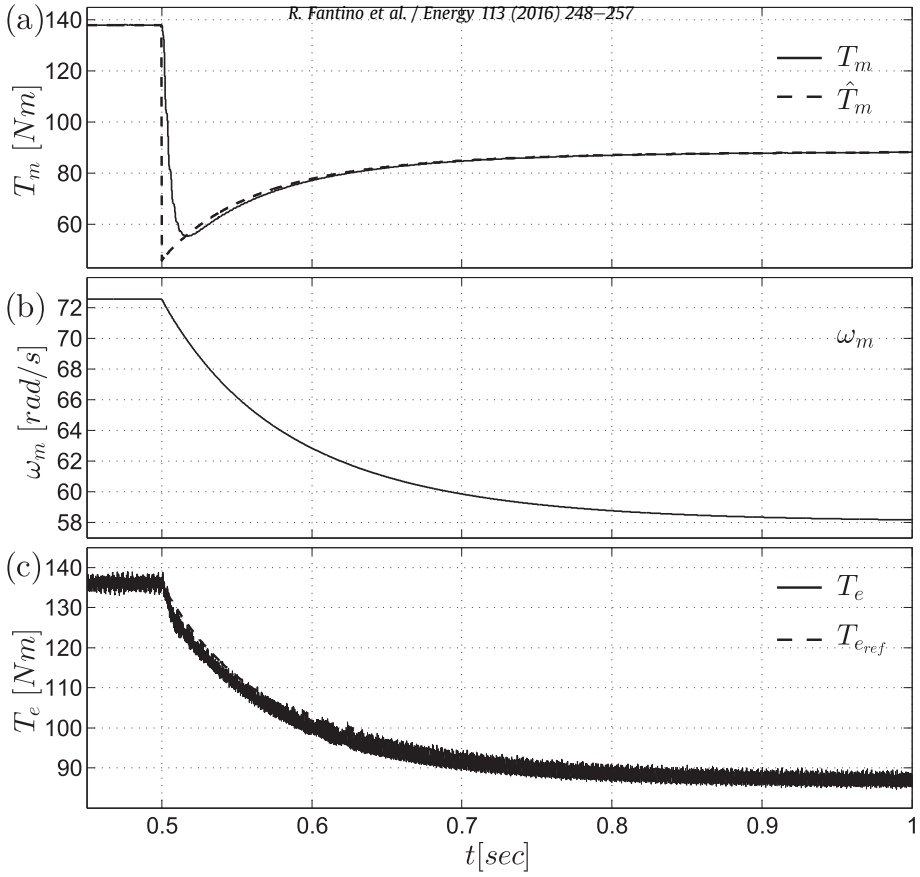

Fig. 4. Simulation of the system (see Fig. 1). Change of wind from 1 to 0.8 pu: (a) T_m and $\hat{T}_m$; (b) ω_m; (c) T_e and $T_{e_{ref}}$.

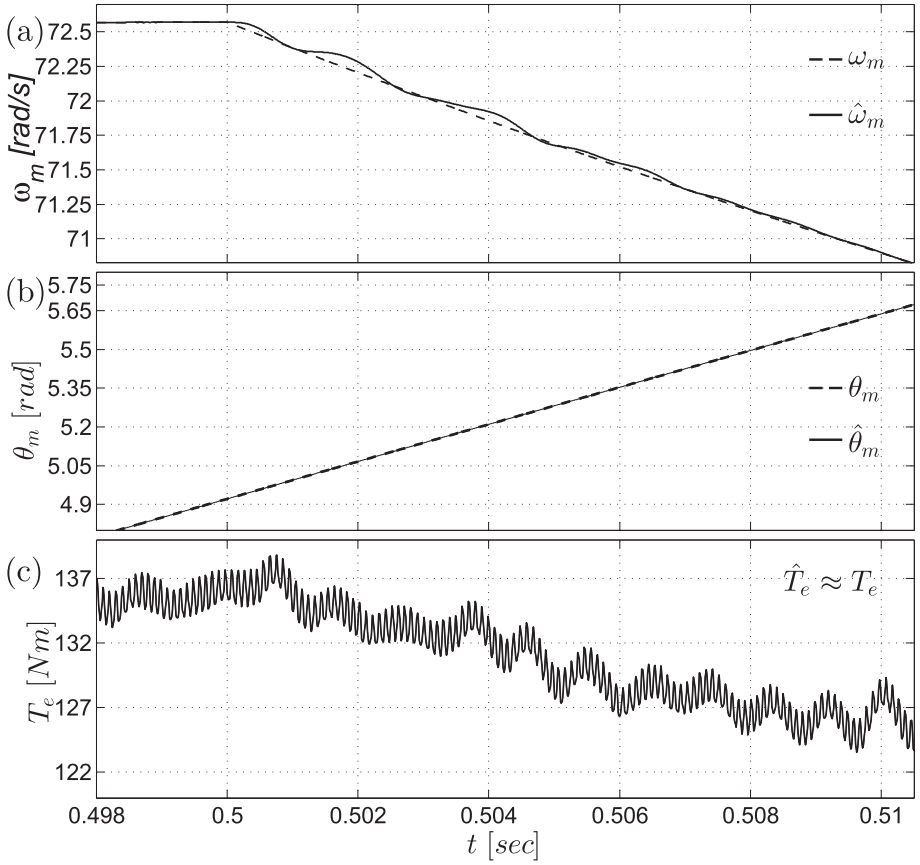

Fig. 5. Simulation of the system (see Fig. 1). Change of wind from 1 to 0.8 pu: (a) ω_m and $\hat{\omega}_m$; (b) θ_m and $\hat{\theta}_m$; (c) $\hat{T}_e \cong T_e$.

The constant value K_{opt} can be obtained using the turbine nominal data.

The block "MPPT Control" is shown in Fig. 3. This block controls the CSR in the WECS shown in Fig. 1. It must be noted that when $(d\omega_m/dt) = 0$ (i.e. steady state) from the PMSG model (Eqn. (1)), the following equation is obtained:

$$T_e\Big|_{\frac{d\omega_m}{dt}=0} = T_m - B\omega_m. \tag{8}$$

By combining Eqn (7) and (8), and using estimated angular speed $\widehat{\omega}_m$ (4), the reference electrical torque for MPPT can be calculated as:

$$T_{e_{ref}} = K_{opt}\widehat{\omega}_m^2 - B\widehat{\omega}_m. \tag{9}$$

It must be noted that to build this reference the speed estimated with the observer was employed, consequently the speed sensor is not needed. This reference must be tracked to guarantee operation on the maximum power curve. The reference is compared with the estimated electrical torque (Eqn. (5)) and the generated error is a PI input, whose output is CSR modulation index m_G, as shown in Fig. 3.

As for CSI (see Fig. 1), a scheme to guarantee that the machine delivers power satisfying the unity power factor condition is proposed. By using estimated rotor position $\widehat{\theta}_m$, the internal EMF electrical angle estimate can be calculated as $\widehat{\theta}_e = P\widehat{\theta}_m$. This angle is considered the initial reference needed for generating the CSR reference angle θ_G. To achieve unity power factor current injection ($i_{G_{\alpha\beta}}$ in-phase with $v_{G_{\alpha\beta}}$), $\widehat{\theta}_e$ is added to the output of a PI controller whose input is given by the cross product between current and voltage vectors $i_{G_{\alpha\beta}} \times v_{G_{\alpha\beta}}$ (see Fig. 3). Nevertheless, this condition can be modified to operate with another power factor value [1,29]. The block 'Sat.' limits the PI output to $-\pi/2<\theta<\pi/2$.

5. Simulation results

In what follows, simulation results obtained for the system described in Fig. 1 are shown. These results were obtained with MATLAB®/SIMULINK®/SimPowerSystems® library [33]. The nominal power of the simulated system is $P_{nom} = 10$ kW. The PMSG [32], wind turbine and observer parameters are listed in Table 1. To reduce the simulation time, in order to visualize the dynamics details of the system variables, a low value of the moment of inertia J was assumed. The parameters of the conversion system (CSR and CSI converters) and LC_R and LC_I filters are shown in Table 2. The SVM of both converters was implemented with a sample time $T_s = 1/f_{SVM}$ [30]. In addition, the parameters of the PI controllers of both converters are also shown in Table 2. In a first test, speed wind v_w was changed from 1pu to 0.8pu (from 12 m/s to 9.6 m/s). As a result, wind turbine power P_m decreases abruptly [see (6)]. This leads to a decrease in the mechanical torque, since $T_m = P_m/\omega_m$. Then, the Turbine-PMSG axle decelerates and its speed (ω_m) decreases. It must be noted that the speed value is estimated by the observer. Consequently, the reference electrical torque (9) decreases as well (see "Control PMP" Figs. 1 and 3). Then, the controller causes a reduction of the electrical torque generated by the PMSG. Thus, extracted current ($i_q = [-i_{G_\alpha}\sin(P\widehat{\theta}_m) + i_{G_\beta}\cos(P\widehat{\theta}_m)]$) is reduced as

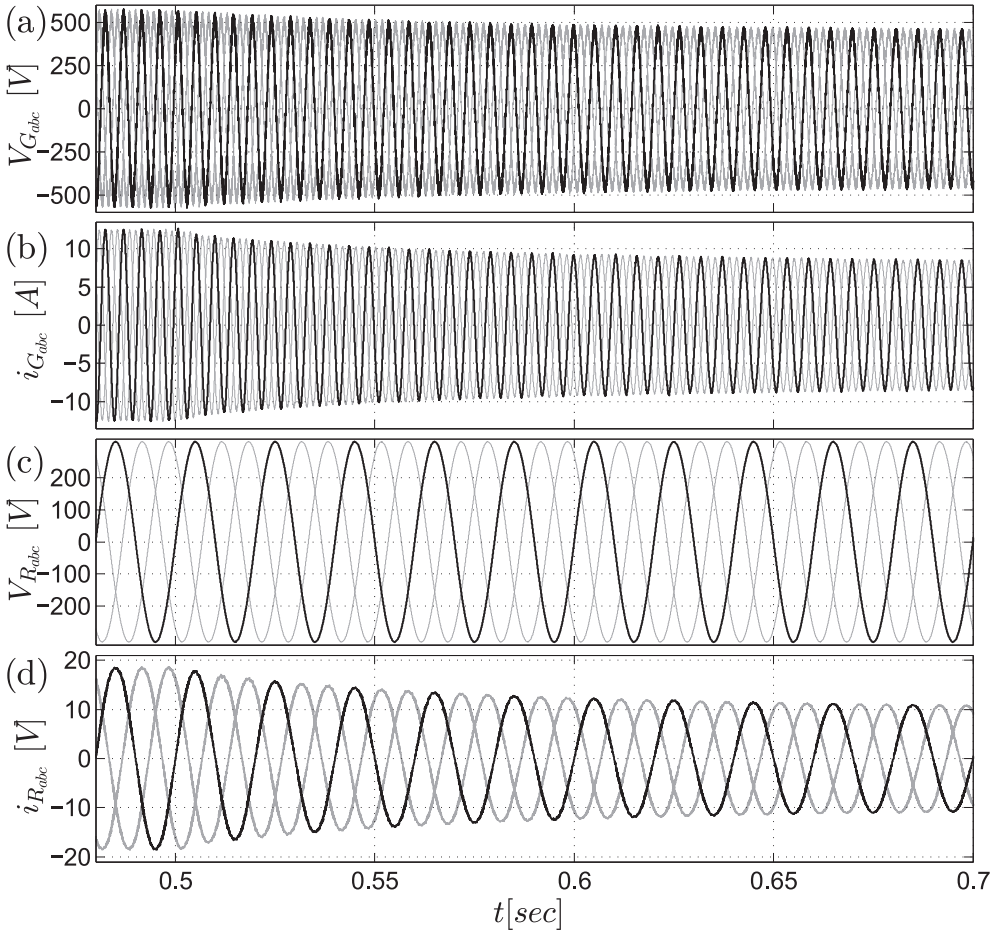

Fig. 6. Simulation of the system (see Fig. 1). Change of wind from 1 to 0.8 pu: (a) $v_{G_{abc}}$; (b) $i_{G_{abc}}$; (c) $v_{R_{abc}}$; (d) $i_{R_{abc}}$.

well, and simultaneously the mechanical torque is increased. This transient behavior ceases when a new steady state point is reached. This new steady state point coincides with the intersection between the turbine torque-speed curve ($v_w = 0.8$ pu) and the maximum power curve. In Fig. 2 the arrowed trajectory shows the described behavior. Figs. 4–6 show the results obtained when a wind step was applied. Fig. 4(a) illustrates mechanical torque T_m behavior and its estimate $\widehat{T}_m$. There is an error because the mechanical torque was assumed slowly varying (see Eqn. (3)). However, if necessary, a more complex model can be included. For instance, a higher-order mechanical torque derivative term could be assumed equal to zero. In such a case, the mechanical torque will be described by a higher-order dynamical system.

Fig. 4(b) shows the change in mechanical speed ω_m from the nominal value $\omega_{m_{nom}} = 72.52 rad/s$ to the steady state value $\omega_m = 58.01$ rad/s. This value corresponds to the turbine maximum power point when it operates with a wind speed equal to $v_w = 0.8$ pu (see Fig. 2). In Fig. 4(c), both electrical torque T_e and its reference torque (Eqn. (9)) are shown. It can be seen that the CSR commutation includes a high frequency ripple in the electrical torque. In addition, it can be noted that the electrical torque abruptly decreases at the beginning because the generator active power also decreases. However, the behavior of PI_{mG} allows to reach the new steady state value (Eqn. (8)) close to the mechanical torque value.

Actual and estimated values needed to implement the control law are shown, in detail, in Fig. 5. In Fig. 5(a) the mechanical speed ω_m and its estimate $\widehat{\omega}_m$ are shown. In Fig. 5(b) rotor position θ_m and its estimate $\widehat{\theta}_m$ are shown. In (c) T_e and its estimate $\widehat{T}_e$ are shown. It can be seen that the observer produces a good estimation of the mechanical angle. This angle is used to obtain $\widehat{T}_e$ (Eqn. (5)), then the electrical torque estimation error is small. The maximum error between the actual mechanical speed and the estimated speed is approximately 0.1 rad/s. Taking into account that the nominal speed is 72.52 rad/s, this error is very small. In addition, this error is corrected by the observer in a short time. Consequently, the control is not affected in a significative way. Thus, it can be concluded that the slowly varying assumption for the mechanical torque does not deteriorate the control performance.

In Fig. 6(a) grid voltage $v_{G_{abc}}$ is shown; and in Fig. 6(b) the behavior of three-phase current ($i_{G_{abc}}$) is shown. In this figure the thick curves correspond to phase "a" both for the PMSG and the grid. It can be seen that, after the wind speed step, has been applied both PMSG current and voltage value are decreased. The current

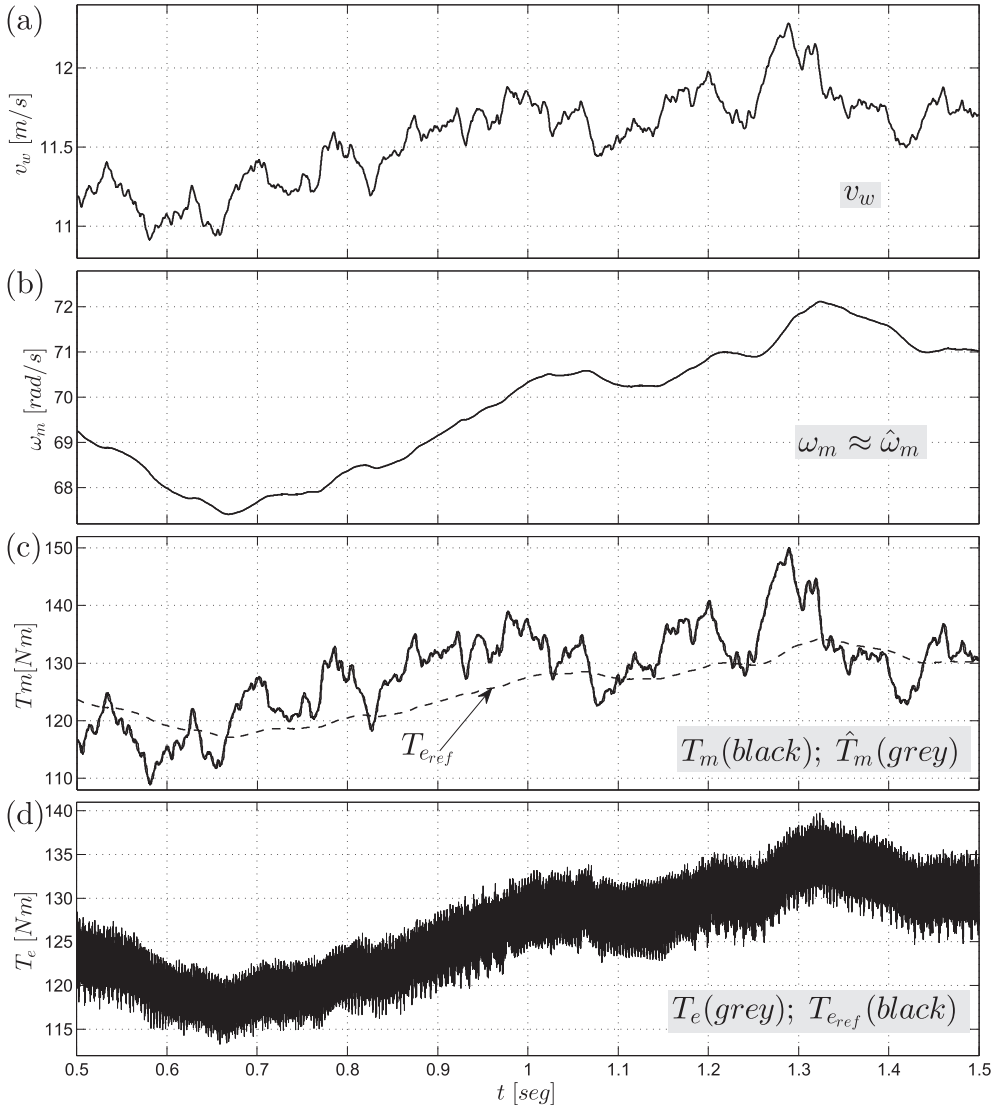

Fig. 7. (a) Realistic wind speed profile. (b) Actual and estimated mechanical speed. (c) Actual and estimated mechanical torque. d) Electrical torque and its reference.

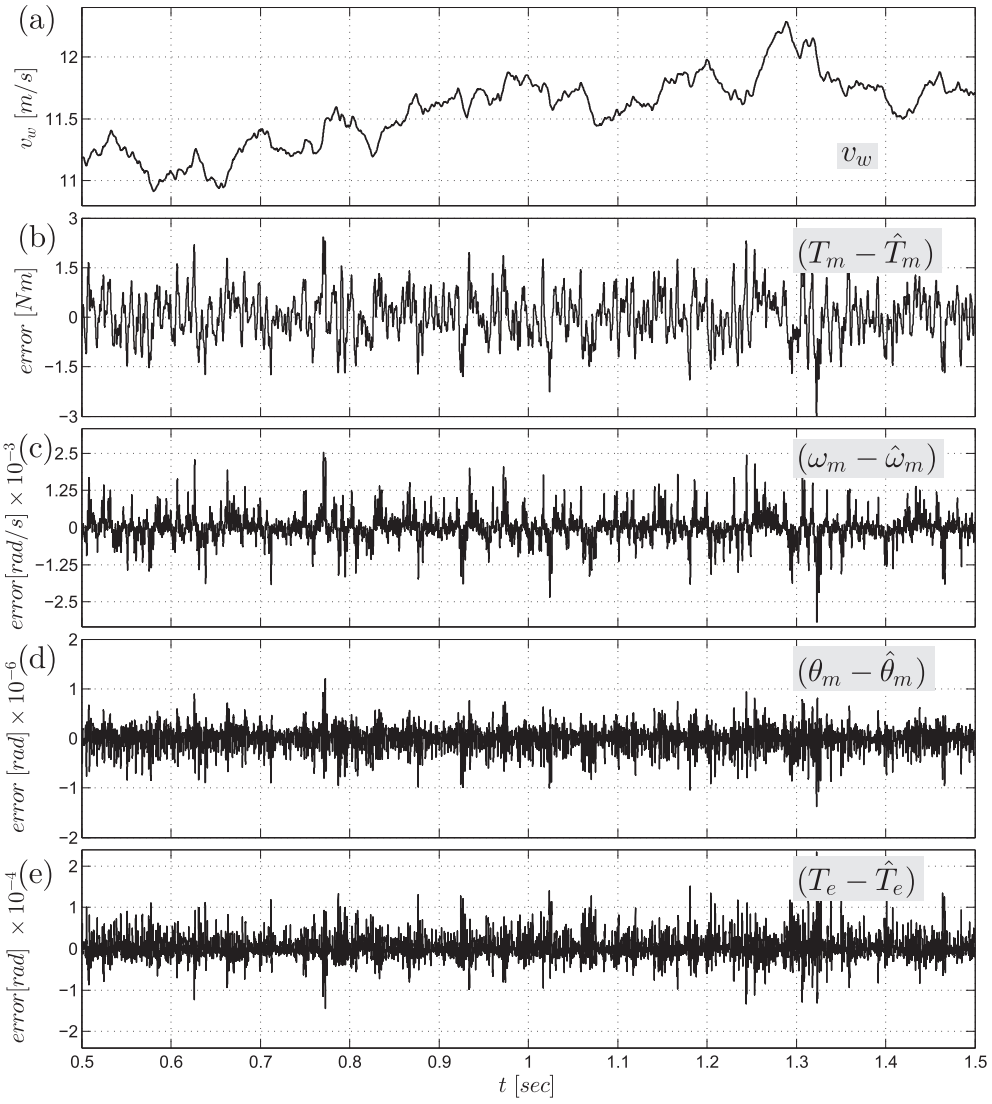

Fig. 8. Estimation errors: (a) Realistic wind speed profile. (b) Mechanical torque estimation error. (c) Mechanical speed estimation error. (d) Mechanical position estimation error. (e) Electrical torque estimation error.

supplied to the grid is decreased as well. It is obviously a consequence of the turbine power reduction. It can be noted that both the PMSG and the grid operate with unity power factor, i.e. currents and voltages are in-phase. It is clear that the system performance is good and the control strategy used to generate the reference angles for CSI and CSR (θ_R and θ_G, respectively) works as expected.

In a second test, a realistic wind speed profile is applied to the system. Fig. 7(a) shows the wind speed profile. This profile is obtained using the von Karman turbulence model [34]. For the time interval in which this wind profile is applied, Fig. 7(b), shows the actual and the estimated mechanical speed, Fig. 7(c) shows the actual and the estimated mechanical torque, and 7(d) shows the electrical torque and its reference. Fig. 8 shows the estimation errors. It can be seen that the proposed controller performs very well. Fig. 8(b) shows the mechanical torque error. This error is less than 5% of the nominal torque. Meaning that the error provoked by assuming a slowly varying torque is broadly tolerable for this application, and consequently a more complex model is not needed. In addition, it can be observed that the other estimation errors are very small.

6. Conclusions

In this work a mechanical sensorless control strategy for a speed variable WECS based on PMSG was introduced. This strategy uses an extended nonlinear observer to estimate the mechanical variables needed to control the PMSG electrical torque. This torque is controlled to track the wind turbine maximum power point.

The main goal behind the proposed strategy is to avoid the use of mechanical sensors in the WECS. This is an important contribution to reduce cost and to increase reliability of the system, mainly in WECS including small size power turbine.

Simulations were introduced to show the performance of the proposed system. It was demonstrated that the system performance is similar to that obtained with controllers that require a mechanical sensor.

Acknowledgements

This work was partially supported by UNS, CONICET and ANPCyT, Argentina.

APPENDIX

In this appendix the methodology for designing the observer is presented. The PMSG model is given by:

$$\begin{bmatrix} \dot{\theta}_m \\ \dot{\omega}_m \\ \dot{i}_{G_\alpha} \\ \dot{i}_{G_\beta} \\ T_e \end{bmatrix} = \begin{bmatrix} \omega_m \\ \frac{T_m}{J} - \frac{B}{J}\omega_m - \frac{T_e}{J} \\ -\frac{R}{L}i_{G_\alpha} - \frac{\lambda_M}{L}P\omega_m \sin(P\theta_m) - \frac{1}{L}v_{G_\alpha} \\ -\frac{R}{L}i_{G_\beta} + \frac{\lambda_M}{L}P\omega_m \cos(P\theta_m) - \frac{1}{L}v_{G_\beta} \\ \frac{3}{2}\lambda_M P\Big[- i_{G_\alpha}\sin(P\theta_m) + i_{G_\beta}\cos(P\theta_m)\Big] \end{bmatrix}, \tag{10}$$

$$\dot{T}_m = 0,$$
$$\boldsymbol{y} = \Big[i_{G_\alpha}\ i_{G_\beta}\Big]^T.$$

In what follows, the following notation will be used: $\theta = P\theta_m$; $\omega = P\omega_m$; $i_\alpha = i_{G_\alpha}$; $i_\beta = i_{G_\beta}$; $v_\alpha = v_{G_\alpha}$; $v_\beta = v_{G_\beta}$; $\lambda_M^{'} = P\lambda_M$; $J^{'} = J/P$; $B^{'} = B/P$.

Then, the model can be written as follows:

$$\begin{bmatrix} \dot{\theta} \\ \dot{\omega} \\ \dot{i}_\alpha \\ \dot{i}_\beta \\ T_e \end{bmatrix} = \begin{bmatrix} \omega \\ \frac{T_m}{J'} - \frac{B'}{J'}\omega - \frac{T_e}{J'} \\ -\frac{R}{L}i_\alpha - \frac{\lambda_M'}{L}\omega \sin\theta - \frac{1}{L}v_\alpha \\ -\frac{R}{L}i_\beta + \frac{\lambda_M'}{L}\omega \cos\theta - \frac{1}{L}v_\beta \\ \frac{3}{2}\lambda_M'\Big[- i_\alpha\sin\theta + i_\beta\cos\theta\Big] \end{bmatrix}, \tag{11}$$

$$\dot{T}_m = 0,$$
$$\boldsymbol{y} = \Big[i_\alpha\ i_\beta\Big]^T.$$

In order to design the observer gains and the adaptation law a nonlinear transformation is proposed. This transformation is: $\xi = [\xi_1\ \xi_2\ \xi_3\ \xi_4\ \xi_5]^T = \left[\frac{\lambda_M'}{L}\omega \sin\theta\ \ -\frac{\lambda_M'}{L}\omega \cos\theta\ i_\alpha\ i_\beta\ T_m\right]^T$. In the new coordinates, the PMSG model is represented by

$$\begin{aligned} \dot{\xi} &= \boldsymbol{A_e}\xi + \boldsymbol{\rho}(\xi) + \boldsymbol{V}\boldsymbol{v}, \\ \boldsymbol{y} &= \boldsymbol{C_e}\xi, \end{aligned} \tag{12}$$

with $\boldsymbol{A_e} = \begin{bmatrix} \boldsymbol{A} & 0 \\ 0 & 0 \end{bmatrix} \varepsilon\, \mathbb{R}^{5\times5}$; $\boldsymbol{C_e} = [\boldsymbol{C}\ 0]\ \varepsilon\, \mathbb{R}^{2\times5}$

$$\boldsymbol{A} = \begin{bmatrix} -B^{'}/J^{'} & 0 & 0 & 0 \\ 0 & -B^{'}/J^{'} & 0 & 0 \\ 1 & 0 & -R/L & 0 \\ 0 & 1 & 0 & -R/L \end{bmatrix}; \qquad \boldsymbol{C} = \begin{bmatrix} 0 & 0 & 1 & 0 \\ 0 & 0 & 1 & 0 \end{bmatrix};$$

$$\boldsymbol{V} = \begin{bmatrix} 0 & 0 & 1/L & 0 & 0 \\ 0 & 0 & 0 & 1/L & 0 \end{bmatrix}^T.$$

$$\boldsymbol{\rho}(\xi) = [m_1\ m_2\ 0\ 0\ 0]^T = \begin{bmatrix} \boldsymbol{m} \\ 0 \end{bmatrix};\ \ \boldsymbol{m}\ \varepsilon\, \mathbb{R}^4 \tag{13}$$

$$\begin{cases} m_1 &= m_{11} + m_{12}\xi_5 \\ &= \dfrac{-kk_1\xi_3\xi_1^2 - kk_1\xi_4\xi_1\xi_2}{\xi_1^2+\xi_2^2} - \sqrt{\xi_1^2+\xi_2^2}\ \dfrac{\xi_2}{k} - \dfrac{k}{J^{'}}\dfrac{\xi_1}{\sqrt{\xi_1^2+\xi_2^2}}\xi_5 \\ m_2 &= m_{21} + m_{22}\xi_5 \\ &= \dfrac{-kk_1\xi_4\xi_2^2 - kk_1\xi_3\xi_1\xi_2}{\xi_1^2+\xi_2^2} - \sqrt{\xi_1^2+\xi_2^2}\ \dfrac{\xi_1}{k} - \dfrac{k}{J^{'}}\dfrac{\xi_2}{\sqrt{\xi_1^2+\xi_2^2}}\xi_5 \end{cases} \tag{14}$$

and $k_1 = 3\phi/2J'$; $k = \lambda_M^{'}/L$; $\boldsymbol{v} = [v_\alpha\ v_\beta]$.

The following observer is proposed for estimating the states in the transformed coordinates.

$$\begin{cases} \dot{\widehat{\xi}} &= \boldsymbol{A_e}\widehat{\xi} + \boldsymbol{\rho}\Big(\widehat{\xi}\Big) + \boldsymbol{V}\boldsymbol{v} + \boldsymbol{G_e}(\boldsymbol{y} - \widehat{\boldsymbol{y}}) + \boldsymbol{l_{ae}}, \\ \boldsymbol{y} &= \boldsymbol{C_e}\widehat{\xi}, \end{cases} \tag{15}$$

where $\boldsymbol{G_e} = [\boldsymbol{G}\ 0]^T$; $\boldsymbol{G}\ \varepsilon\, \mathbb{R}^{4\times2}$; $\boldsymbol{l_{ae}} = [0\ l_a]^T$; $l_a\ \varepsilon\, \mathbb{R}$ is the adaptation law.

$$\begin{aligned} \boldsymbol{e_\xi} &= \xi - \widehat{\xi}, \\ \dot{\boldsymbol{e}}_\xi &= \begin{bmatrix} \boldsymbol{A} - \boldsymbol{GC} & 0 \\ 0 & 0 \end{bmatrix}\boldsymbol{e_{xi}} + \Delta\boldsymbol{\rho} - \boldsymbol{l_{ae}}, \end{aligned} \tag{16}$$

with $\Delta\boldsymbol{\rho} = \boldsymbol{\rho}(\xi) - \boldsymbol{\rho}\Big(\widehat{\xi}\Big) = \begin{bmatrix} \Delta\boldsymbol{m} \\ 0 \end{bmatrix}$; $\Delta\boldsymbol{m}\ \varepsilon\, \mathbb{R}^4$

$$\Delta\boldsymbol{m} = \begin{bmatrix} \Delta m_{11} + \Delta m_{12}\xi_5 + \Delta m_{12}\Big(\widehat{\xi}\Big)e_{\xi_5} \\ \Delta m_{21} + \Delta m_{22}\xi_5 + \Delta m_{22}\Big(\widehat{\xi}\Big)e_{\xi_5} \\ 0 \\ 0 \end{bmatrix}. \tag{17}$$

The adaptation law and the gain matrix must be chosen to guarantee the convergence to zero of the estimation error. A Lyapunov candidate function is chosen. This function is given by:

$$\boldsymbol{V} = \boldsymbol{e}_\xi^T\boldsymbol{P_e}\,\boldsymbol{e}_\xi;\ \ \boldsymbol{P_e} = \begin{bmatrix} \boldsymbol{P} & 0 \\ 0 & I \end{bmatrix}. \tag{18}$$

The Laypunov function time derivative results

$$\begin{aligned} \dot{\boldsymbol{V}} &= \boldsymbol{e}_\nu^T\Big(\boldsymbol{A}_\boldsymbol{c}^T\boldsymbol{P} + \boldsymbol{P}\boldsymbol{A_c}\Big)\boldsymbol{e}_\nu + 2\boldsymbol{e}_\nu^T\boldsymbol{P}\Delta\boldsymbol{m} - 2l_a e_{\xi_5} \\ \boldsymbol{e}_\nu &= \Big[e_{\xi_1}\ e_{\xi_2}\ e_{\xi_3}\ e_{\xi_4}\Big]^T;\ \ \boldsymbol{A_c} = (\boldsymbol{A} - \boldsymbol{GC}). \end{aligned} \tag{19}$$

By choosing matrix Q to satisfy the following Lyapunov equation

$$\boldsymbol{A}_\boldsymbol{c}^T\boldsymbol{P} + \boldsymbol{P}\boldsymbol{A_c} = -Q;\ Q > 0, \tag{20}$$

then, the following equality is obtained.

$$\dot{\boldsymbol{V}} = -\boldsymbol{e}_\nu^T Q\,\boldsymbol{e}_\nu + 2\boldsymbol{e}_\nu^T\boldsymbol{P}\Delta\boldsymbol{m} - 2l_a e_{\xi_5}. \tag{21}$$

This equation suggests to use the following adaption law: $l_a = \boldsymbol{h}^T(\widehat{\xi})\boldsymbol{P}\,\boldsymbol{e}_\nu$; con $\boldsymbol{h}^T = [m_{12}\ m_{22}\ 0\ 0]$. Then, the following inequality is satisfied for the Lyapunov function time derivative

$$\dot{\boldsymbol{V}} \le (\ -q + 2pL_1 + 2pL_2||\xi_5||)\Big|\Big|e_\nu\Big|\Big|^2. \tag{22}$$

In this inequality, q is the minimum eigenvalue of Q; p is the maximum eigenvalue of $\boldsymbol{P}$; L_1 and L_2 are the Lipschitz constant of m_1 and m_2, respectively.

By assuming that $||\xi_5||$ is bounded, when $\sigma = -q + 2pL_1 + 2pL_2||\xi_5|| < 0$ the estimation error converges to zero. It must be noted that e_{ξ_1} and e_{ξ_2} cannot be used in the adaptation law, because ξ_1 and ξ_2 are not measurable. In original coordinates, the adaptation law built from the measured variables results:

$$l_a' = -k_1 \sin\left(P\widehat{\theta}_m\right)\left(i_\alpha - \widehat{i}_\alpha\right) + k_2 \cos\left(P\widehat{\theta}_m\right)\left(i_\beta - \widehat{i}_\beta\right). \tag{23}$$

Then, coming back to the original coordinates the observer description is given by (4).

References

[1] Wu B, Lang Y, Zargari N, Kouro S. Power conversion and control of wind energy systems. Wiley-IEEE Press; 2011.

[2] Nguyen TH, Lee D-C. A novel current control scheme of grid converters for small pmsg wind turbines under grid voltage distortion. In: Power electronics and machines in wind applications (PEMWA), 2012 IEEE; July 2012. p. 1–6.

[3] Espinoza J, Joos G. A current-source-inverter-fed induction motor drive system with reduced losses. Ind Appl IEEE Trans 2012:1–6.

[4] Enjeti P, Ziogas P, Lindsay J. A current source pwm inverter with instantaneous current control capability. Ind Appl IEEE Trans 1991;27:582–8.

[5] Phillips KP. Current-source converter for ac motor drives. Ind Appl IEEE Trans 1979;IA-8:445–52.

[6] Dai J, Xu D, Wu B. A novel control scheme for current-source-converter-based pmsg wind energy conversion systems. Power Electron IEEE Trans April 2009;24:963–72.

[7] Nikolic A, Jeftenic B. Current source converter topologies for pmsg wind turbine applications. In: Power electronics and motion control conference (EPE/PEMC), 2010 14th international; Sept 2010. S14–27. S14–32.

[8] Popat M, Wu B, Zargari N. A novel decoupled interconnecting method for current-source converter-based offshore wind farms. Power Electron IEEE Trans Oct 2012;27:4224–33.

[9] Yin X-x, Lin Y-g, Li W, Gu Y-j, Liu H-w, Lei P-f. A novel fuzzy integral sliding mode current control strategy for maximizing wind power extraction and eliminating voltage harmonics. Energy 2015;85:677–86.

[10] Alizadeh M, Shokri Kojori S. Augmenting effectiveness of control loops of a pmsg (permanent magnet synchronous generator) based wind energy conversion system by a virtually adaptive pi (proportional integral) controller. Energy 2015;91:610–29.

[11] Elnaggar M, Abdel Fattah H, Elshafei A. Maximum power tracking in wecs (wind energy conversion systems) via numerical and stochastic approaches. Energy 2014;74:651–61.

[12] Belmokhtar K, Doumbia M, Agbossou K. Novel fuzzy logic based sensorless maximum power point tracking strategy for wind turbine systems driven dfig (doubly-fed induction generator). Energy 2014;76:679–93.

[13] Inoue Y, Morimoto S, Sanada M. Control method for direct torque controlled pmsg in wind power generation system. In: Electric machines and drives conference, 2009. IEMDC '09. IEEE international; May 2009. p. 1231–8.

[14] Zhang Z, Zhao Y, Qiao W, Qu L. A space-vector-modulated sensorless direct-torque control for direct-drive pmsg wind turbines. Ind Appl IEEE Trans July 2014;50:2331–41.

[15] Orlando N, Liserre M, Monopoli V, Dell'Aquila A. Speed sensorless control of a pmsg for small wind turbine systems. In: Industrial electronics, 2009. ISIE 2009. IEEE international symposium on; July 2009. p. 1540–5.

[16] Abdelkafi A, Krichen L. New strategy of pitch angle control for energy management of a wind farm. Energy 2011;36:1470–9.

[17] Hossain MM, Ali MH. Future research directions for the wind turbine generator system. Renew Sustain Energy Rev 2015;49:481–9.

[18] Orlando NA, et al. A survey of control issues in pmsg-based small wind-turbine systems. Ind Inf IEEE Trans 2013;9(3):1211–21.

[19] Thongam J, Bouchard P, Beguenane R, Fofana I, Ouhrouche M. Sensorless control of pmsg in variable speed wind energy conversion systems. In: Power electronics conference (IPEC), 2010 international; June 2010. p. 2254–9.

[20] Huang K, Zheng L, Huang S, Xiao L, Li W. Sensorless control for direct-drive pmsg wind turbines based on sliding mode observer. In: Electrical machines and systems (ICEMS), 2011 international conference on; Aug 2011. p. 1–5.

[21] Liu W, Chen L, Ou J, Cheng S. Simulation of pmsg wind turbine system with sensor-less control technology based on model reference adaptive system. In: Electrical machines and systems (ICEMS), 2011 international conference on; Aug 2011. p. 1–3.

[22] Chou Y, Nian H. Sensorless control of pmsg based on dual two-level inverter open winding configuration for wind turbines. In: Electrical machines and systems (ICEMS), 2012 15th international conference on; Oct 2012. p. 1–6.

[23] Jaramillo-Lopez F, Kenne G, Lamnabhi-Lagarrigue F. A novel online training neural network-based algorithm for wind speed estimation and adaptive control of pmsg wind turbine system for maximum power extraction. Renew Energy 2016;86:38–48.

[24] Urtasun A, Sanchis P, San Martín I, López J, Marroyo L. Modeling of small wind turbines based on pmsg with diode bridge for sensorless maximum power tracking. Renew energy 2013;55:138–49.

[25] Urtasun A, Sanchis P, Marroyo L. Small wind turbine sensorless mppt: robustness analysis and lossless approach. Ind Appl IEEE Trans 2014;50(6):4113–21.

[26] Aubrée R, Auger F, Macé M, Loron L. Design of an efficient small wind-energy conversion system with an adaptive sensorless mppt strategy. Renew Energy 2016;86:280–91.

[27] Lončarek T, Lešić V, Vašak M. Increasing accuracy of kalman filter-based sensorless control of wind turbine pm synchronous generator. In: Industrial technology (ICIT), 2015 IEEE international conference on; March 2015. p. 745–50.

[28] Solsona J, Valla M, Muravchik C. Nonlinear control of a permanent magnet synchronous motor with disturbance torque estimation. Energy Convers IEEE Trans Jun 2000;15:163–8.

[29] Dai J, Xu D, Wu B. A novel control system for current source converter based variable speed pm wind power generators. In: Power electronics specialists conference, 2007. PESC 2007. IEEE; 2007. p. 1852–7.

[30] Pham D, Huang S, Huang K. Modeling and simulation of current source inverters with space vector modulation. In: Electrical machines and systems (ICEMS), 2010 international conference on; Oct 2010. p. 320–5.

[31] Orando N, Mastromauro R, Liserre M, Dell'Aquila A. Grid voltage support by means of a small wind turbine system. In: Industrial electronics, 2008. IECON 2008. 34th annual conference of IEEE; Nov 2008. p. 2178–83.

[32] Shariatpanah H, Fadaeinedjad R, Rashidinejad M. A new model for pmsg-based wind turbine with yaw control. IEEE Trans Energy Convers Dec 2013;28:929–37.

[33] MATLAB®, version 8.1.0.604 (R2013a). Natick, Massachusetts: The MathWorks Inc; 2013.

[34] Nichita C, Luca D, Dakyo B, Ceanga E. Large band simulation of the wind speed for real time wind turbine simulators. Energy Convers IEEE Trans 2002;17(4):523–9.